HHS Public Access

Author manuscript

J Geophys Res Atmos. Author manuscript; available in PMC 2022 November 03.

Published in final edited form as:

J Geophys Res Atmos. 2013 October 16; 118(19): 11242–11255. doi:10.1002/jgrd.50862.

High-resolution MODIS aerosol retrieval during wildfire events in California for use in exposure assessment

Sean M. Raffuse[1], **Michael C. McCarthy**[1], **Kenneth J. Craig**[1], **Jennifer L. DeWinter**[1], **Loayeh K. Jumbam**[1,2], **Scott Fruin**[3], **W. James Gauderman**[3], **Frederick W. Lurmann**[1]

[1]Sonoma Technology, Inc., Petaluma, California, USA.

[2]Now at Esri, Redlands, California, USA.

[3]Keck School of Medicine, University of Southern California, Los Angeles, California, USA.

Abstract

Retrieval of aerosol optical depth (AOD) from the Moderate Resolution Imaging Spectroradiometer (MODIS) using the Collection 5 (C005) algorithm provides large-scale (10 × 10 km) estimates that can be used to predict surface layer concentrations of particulate matter with aerodynamic diameter smaller than 2.5 μm ($PM_{2.5}$). However, these large-scale estimates are not suitable for identifying intraurban variability of surface $PM_{2.5}$ concentrations during wildfire events when individual plumes impact populated areas. We demonstrate a method for providing high-resolution (2.5 km) kernel-smoothed estimates of AOD over California during the 2008 northern California fires. The method uses high-resolution surface reflectance ratios of the 0.66 and 2.12 μm channels, a locally derived aerosol optical model characteristic of fresh wildfire plumes, and a relaxed cloud filter. Results show that the AOD derived for the 2008 northern California fires outperformed the standard product in matching observed aerosol optical thickness at three coastal Aerosol Robotic Network sites and routinely explained more than 50% of the variance in hourly surface $PM_{2.5}$ concentrations observed during the wildfires.

1. Introduction

A combination of drought conditions and a large number of lightning strikes started more than 1000 wildfires in northern California on 20–21 June 2008. These wildfires emitted significant amounts of smoke and had a dramatic impact on air quality throughout northern and central California over the next 2 months. The fires occurred in the mountainous areas that surround California's Central Valley, including the Sierra Nevada Mountains, the Klamath Mountains, and the North Coast Range. Analysis of the fires indicated that between 1.5 and 2 million acres were burned, producing approximately 540,000 to 725,000 t of primary particulate matter with aerodynamic diameter smaller than 2.5 μm ($PM_{2.5}$) [Reid et al., 2009]. Meteorological conditions conducive to smoke accumulation led to unhealthful air quality and a large number of exceedances of the National Ambient Air Quality

Corresponding author: S. M. Raffuse, Sonoma Technology, Inc., 1445 N. McDowell Blvd., Suite D, Petaluma, CA 94954-65, USA. (sraffuse@sonomatech.com).

Additional supporting information may be found in the online version of this article.

Standards throughout the region [California Air Resources Board, 2012]. Metropolitan regions including Sacramento (population 2.5 million), Fresno (0.9 million), and the San Francisco Bay Area (7.5 million) were impacted by the smoke. During the 8 week event, meteorological conditions led to repeated multiday episodes of intense smoke separated by one or more relatively clean days. Forty monitoring sites recorded $PM_{2.5}$ observations in central and northern California during the fire events. Hourly observations routinely exceeded 100 $\mu g/m^3$ at monitoring sites on 23–27 June 2008 and 9–10 July 2008.

Phase modulation (PM) derived from biomass burning has been associated with a variety of health outcomes, including respiratory morbidity [Delfino et al., 2009; Künzli et al., 2006; Naeher et al., 2007; Schreuder et al., 2006; Sood et al., 2010], but public health impact assessments of large wildfire events are hampered by the paucity of air quality data. Unlike typical regional pollution episodes, wildfire events can produce distinct plumes of dense smoke with high $PM_{2.5}$ concentrations (>200 $\mu g/m^3$) within a few kilometers of areas where $PM_{2.5}$ concentrations remain at background levels [Castanho et al., 2008; Wu et al., 2006]. For epidemiological studies to evaluate health effects associated with these wildfire events, the spatial and temporal distribution of $PM_{2.5}$ concentrations in the smoke plumes must be accurately characterized.

Surface $PM_{2.5}$ monitoring stations in central and northern California have limited spatial coverage, but satellite measurements of aerosol optical depth (AOD) have the potential to augment the surface monitoring network observations. The Moderate Resolution Imaging Spectrometer (MODIS) AOD data have been used in a variety of studies in recent years to estimate surface PM concentrations [e.g., Castanho et al., 2008; Engel-Cox et al., 2004a, 2004b; Gupta et al., 2006; Liu et al., 2007; Oo et al., 2010; Wu et al., 2006]. Initial studies compared standard AOD products provided by the National Aeronautics and Space Administration (NASA) to surface concentrations over the eastern United States [Engel-Cox et al., 2004a, 2004b; Liu, 2004].

The standard MODIS Collection 5 AOD algorithm product provided by NASA is typically used to characterize global aerosol loading. Several aspects of the standard AOD product limit its usefulness for estimating surface $PM_{2.5}$ concentrations during wildfire episodes. First, the standard AOD product is provided at relatively low spatial resolution (10 × 10 km). Higher spatial resolution AOD is highly desirable for characterizing intraurban aerosol variability, as is preferable for epidemiological studies. Second, methods used by the standard AOD product algorithm underestimate the surface reflectance ratio between the visible and shortwave infrared channels in urban areas [Oo et al., 2010]. Because urban surface brightness is heterogeneous over short spatial scales, surface reflectance ratios must be produced at high resolution to avoid underpredicting surface brightness [Castanho et al., 2007, 2008; Li et al., 2005; Oo et al., 2010]. Underestimating surface brightness ratios results in significant overprediction of AOD retrieved from top-of-atmosphere (TOA) reflectance [Castanho et al., 2007]. This is especially problematic for areas of the western United States where dry surface conditions lead to bright surfaces [Engel-Cox et al., 2004a, 2004b]. This contributes to the poor performance of MODIS AOD as a predictor of surface $PM_{2.5}$ concentrations in the western United States under nonwildfire conditions [Engel-Cox et al., 2004a, 2004b; Green et al., 2009; Hu, 2009]. Third, the clean background aerosol

optical model currently used for the western United States in the standard AOD product algorithm is not appropriate for smoke events [Omar et al., 2005; Remer et al., 2009]. A biomass burning aerosol optical model is more representative of regional aerosol scattering and absorption properties during smoke events. Finally, the cloud mask algorithm used in the standard AOD product screens thick smoke plumes as clouds. It is necessary to relax the standard product cloud filters to retain valid smoky pixels that are typically screened in the standard AOD product.

We developed a high-resolution (2.5 × 2.5 km) AOD product capable of producing reliable estimates of surface $PM_{2.5}$ concentrations during wildfire episodes. We combined methods pioneered by numerous other studies [Castanho et al., 2007; Drury et al., 2008; Omar et al., 2005; Oo et al., 2010; van Donkelaar et al., 2011] with our own modifications to account for the unique topography, geography, and aerosol characteristics of the 2008 northern California fires. We utilize the native resolution (500 m in some channels) of the MODIS instrument and perform all processing on a 500 m resolution analysis grid. The final AOD values are then smoothed by using a trimmed mean over a 2.5 km kernel. This spatial smoothing is essential to reduce the influence of instrument noise on high-resolution estimates.

Our approach addresses important limitations of the standard AOD product by (1) developing high-resolution AOD capable of resolving distinct plumes of dense wildfire smoke, (2) developing high-resolution surface reflectance ratio maps to improve the characterization of surface brightness over urban areas, (3) relaxing the standard AOD product cloud mask to minimize false cloud detects in heavy aerosol, and (4) developing appropriate aerosol optical properties from biomass burning aerosol observed in California. This paper describes the methodology and its application to the 2008 northern California fire events. $PM_{2.5}$ estimates for the 2008 fires are provided, along with potential implications for population exposure during the events.

2. Methods

To derive AOD at 0.55 μm ($\tau_{0.55}$) at high-spatial resolution over California during heavy smoke events, we employed a single-channel inversion following the method of Castanho et al. [2008]. The method used the observed TOA reflectance at 0.66 μm and sun-target-sensor angles, along with derived aerosol optical properties and surface reflectance at 0.66 μm. A cubic spline was used to fit a look-up table relating the 0.66 reflectance to AOD at 0.55 μm for the given viewing conditions. All processing was performed on a 500 m resolution grid. Final AOD values were then smoothed by using a trimmed mean over a 2.5 km kernel. The Remer et al. [2009] cloud mask algorithm with relaxed screening criteria from van Donkelaar et al. [2011] was used to increase coverage of the AOD retrieval. The following subsections describe the key aspects of the MODIS data preparation and AOD processing algorithm. A schematic depiction of the method components is shown in Figure 1.

2.1. Data Acquisition and Preparation

Raw Level 1b MODIS radiance data and corresponding geolocation data from the Terra and Aqua satellites were obtained from the NASA Goddard Space Flight Center Level 1 and

Atmosphere Archive and Distribution System (http://ladsweb.nascom.nasa.gov/). Data from 24 June to 31 July 2008 were acquired to cover the time period substantially impacted by the 2008 northern California wildfire outbreak. In addition, data from the same months of 2009 were acquired to develop surface reflectance maps. Vegetation color was similar during the summers of 2008 and 2009, but atmospheric smoke loading was less prominent in 2009, providing additional clean atmosphere days for deriving surface reflectance values.

MODIS reflectance data contain atmospheric trace gas signals due to absorption by water vapor, ozone, and carbon dioxide. These signals must be removed prior to AOD estimation. Corrections for these gasses were applied to the raw Level 1b MODIS radiance data using the same correction methodology applied in the MOD04/MYD04 collection 5 L2 version 2.0 aerosol algorithm [Remer et al., 2009].

Gas-corrected MODIS Level 1b reflectance data at the granule level were warped, subset, and spliced together to produce georeferenced images on a unified Universal Transverse Mercator analysis grid at 500 m resolution. These georeferenced images allowed for pixel-level comparisons across days using standardized locations. The analysis grid covered most of California and included all regions impacted by the 2008 northern California wildfire outbreak. Solar and satellite angle data from their native 1 km resolution were also geoprocessed for the unified analysis grid to provide one-to-one correspondence between reflectance pixels and the sun-sensor angles. These daily gas-corrected MODIS reflectance data were the basis of subsequent analysis.

Water vapor and ozone data for the gas corrections were acquired from the Space Science and Engineering Center at the University of Wisconsin-Madison. Water vapor data were generated from the National Centers for Environmental Prediction 1° by 1° Global Data Assimilation System 6-hourly meteorological analysis [Derber et al., 1991], while column ozone data were generated from the National Atmospheric and Oceanic Administration Total Ozone Analysis using SBUV/2 and TOVS 1° by 1° daily global ozone analysis [Bhartia et al., 1996; Neuendorffer, 1996]. We used globally fixed CO_2 optical depths prescribed in the MODIS Collection 5 operational AOD code. Data gaps were filled using climatology for first guess profiles.

2.2. Cloud Mask Relaxation

Identifying cloud-contaminated pixels is an important part of the AOD retrieval, since AOD inversion is not possible in the presence of clouds. The cloud mask algorithm implemented for MOD04 and MYD04 leaves residual cloud contamination, and masking clouds without masking heavy aerosol remains a difficult challenge [Remer et al., 2009]. We analyzed failed AOD retrievals over California from the MODIS AOD product and found they were often triggered by false cloud contamination, even in clean, cloudless conditions. We also found that the current cloud mask mistakes thick aerosol plumes for clouds, as did van Donkelaar et al. [2011].

The MODIS AOD product cloud mask is a combination of brightness and spatial variability tests at 0.47 and 1.38 μm, as described by Remer et al. [2009]. Van Donkelaar et al. [2011] relaxed this cloud mask algorithm to increase coverage of the AOD retrieval for studying

the 2010 Moscow, Russia, wildfire smoke events. We applied the same modifications to our cloud mask for this study of California wildfire smoke. First, the maximum allowed spatial variability of 0.47 μm was relaxed from 0.0025 to 0.005 to reduce the number of heavy aerosol pixels masked as cloud. Second, if the 0.47 μm threshold of 0.005 was exceeded but the 2.12 μm was less than 0.025, a pixel was classified as aerosol, as fine mode aerosol is transparent at 2.12 μm relative to cloud or dust [Kaufman and Fraser, 1997]. This relaxed cloud mask improved the coverage of our AOD retrievals for California wildfire events, while reducing spurious false cloud retrievals over highly textured land surfaces.

2.3. Surface Reflectance Ratio Adaptation

The determination of the aerosol contribution to TOA reflectance requires subtraction of the signal coming from surface reflectance. We derived the surface reflectance at 0.66 μm using the TOA reflectance at 2.13 μm and a 0.66/2.13 surface reflectance ratio ($\xi_{0.66}$). As reported in Oo et al. [2010], we found that the method used by the MOD04 Collection 5 algorithm underestimates $\xi_{0.66}$ in the urban areas of our domain, resulting in an overestimation of AOD. Therefore, we applied an approach developed by Drury et al. [2008] to calculate $\xi_{0.66}$ over our study domain and season (June–July). On clean (i.e., low PM) days when the atmosphere is optically thin, nadir-scaled atmospheric reflectance varies linearly with AOD. This allowed us to use a linear equation of the form $y = mx + b$, where x is the 2.13 μm nadir-scaled reflectance and y is the 0.66 μm nadir-scaled reflectance. Under this approach, a scatterplot of y versus x for multiple days and view angles for the same location has a lower envelope with a slope (m) of $\xi_{0.66}$. Details of the derivation are provided in Drury et al. [2008].

To determine $\xi_{0.66}$ from the scatterplots, we first binned the 2.13 μm nadir-scaled reflectances (x) into sequential groups of five and retained the lowest two values in each bin. We then applied a reduced major axis regression on the remaining values to calculate the slope. Because our time period of interest (June–August 2008) was dominated by pervasive high-smoke aerosol loadings, we used MODIS data from the same season in 2009 to develop the scatterplots and derive surface reflectance ratios. Figure 2 shows a map of the derived $\xi_{0.66}$ values. Our values range from 0.3 to near 1, with the lowest values occurring in areas of sparse vegetation and the highest values in coastal forests and the Sierra Nevada Mountains. The $\xi_{0.66}$ of urban areas is between 0.65 and 0.9. The dynamic range of these values is greater than those used in the MOD04 Collection 5 algorithm.

2.4. Aerosol Optical Model Development

We localized the AOD algorithm by developing a set of aerosol optical properties using Aerosol Robotic Network (AERONET) [Holben et al., 1998] sun photometer measurements from 2003 to 2007 for five sites in California: La Jolla, University of California at Los Angeles, Santa Barbara, Table Mountain, and Fresno. AERONET provides retrievals of aerosol optical properties such as size distribution, complex index of refraction, single scattering albedo, and phase functions by inverting the sun photometer radiance data [Dubovik and King, 2000]. We used Level 2.0-validated AERONET data, which are cloud screened and quality controlled.

We performed a cluster analysis on AERONET data from the five selected sites, following the method presented in Omar et al. [2005], to identify unique clusters of aerosol data. Aerosol optical properties from the five AERONET sites fell into two dominant and distinct clusters: aerosol typical of polluted air in California (called typical), and a biomass burning aerosol (called biomass).

Figure S1 in the supporting information shows a comparison of average aerosol size distributions from the California AERONET sites with the global aerosol models currently incorporated in MODIS standard aerosol products that most resemble California. In the global MODIS-processed data, the rural/background aerosol model is used for the entire western United States ("Omar Western"). The size distribution of the biomass aerosol from California is different from the size distribution in the *Omar et al*. biomass model. Compared to aged biomass aerosols, fresh biomass aerosols are dominated by smaller particles, and the days identified as biomass dominated in our California data generally included fresh emissions from nearby fires. Differences in size distributions between fresh and aged biomass aerosol have also been observed in Amazonia fires [Martins et al., 1998].

2.5. AOD Retrieval

AOD retrieval is based on the single-channel inversion method of Castanho et al. [2008]. A radiative transfer model (RTM) was used to precompute a look-up table (LUT) of relationships between TOA reflectance at 0.66 μm and AOD at 0.55 μm ($\tau_{0.55}$) for our AERONET-based aerosol models at a variety of sun-sensor geometries and surface reflectances (Table 1). For this work, the LUT was based on over 2 million simulations using the "Second Simulation of a Satellite Signal in the Solar Spectrum" (6S) RTM version 1.1 [Kotchenova and Vermote, 2007; Kotchenova et al., 2006]. The 6S RTM is based on the method of successive orders of scattering approximations [Vermote et al., 1997] and includes polarization effects through calculation of the four Stokes vector components. It has been extensively tested, and it currently underlies the MODIS operational atmospheric correction algorithm [Vermote et al., 2002]. Our simulations assume homogeneous, Lambertian, and nonpolarizing surface reflectance. Aerosol size distribution and refractive indices from both aerosol models were provided as input for one-time executions of the 6S Mie scattering code, which produced extinction coefficients, asymmetry factors, and aerosol phase functions used by the bulk RTM simulations.

Figure 3 shows a family of relationships between $\tau_{0.55}$ and TOA reflectance produced by a series of 6S RTM simulations with different surface reflectances for a typical MODIS sun-sensor geometry. These curves are consistent with theoretical considerations discussed by Fraser and Kaufman [1985]. For dark surfaces, aerosol loading increases TOA reflectance, and the relationship between $\tau_{0.55}$ and TOA reflectance is well defined. For extremely bright surfaces, aerosol loading reduces TOA reflectance, and the relationship between $\tau_{0.55}$ and TOA reflectance is well defined. For moderately bright surfaces near the critical reflectance, aerosol loading has little impact on TOA reflectance, and the relationship between $\tau_{0.55}$ and TOA reflectance is poorly defined [Fraser and Kaufman, 1985; Kaufman, 1987]. AOD estimation over surfaces near the critical reflectance is therefore difficult, and several tests are applied in the AOD inversion process to catch these occurrences. Most urban surfaces

in our analysis area fall below the critical reflectance and are therefore dark enough for accurate AOD inversion over a large portion of the analysis grid.

AOD is determined using TOA reflectance at 2.12 and 0.66 μm and the surface reflectance ratio computed from our Drury et al. [2008] analysis. Assuming that fine mode aerosol is approximately transparent at 2.12 μm relative to cloud or dust [Kaufman et al., 2002; Kaufman and Fraser, 1997], the surface reflectance at 0.66 μm can be derived by scaling the TOA reflectance at 2.12 μm by the reflectance ratio [Drury et al., 2008]. For water surface pixels, we use a baseline surface reflectance of 0.002 instead of deriving it from reflectance ratios, which are only applicable over land. LUT data from the RTM are interpolated to the proper sun-sensor geometry and 0.66 μm surface reflectance to generate a curve of $\tau_{0.55}$ as a function of TOA reflectance. This $\tau_{0.55}$ curve is fit to a cubic spline to determine AOD for the satellite TOA reflectance. AOD retrievals were rejected from curve fits that produced correlation coefficients smaller than 0.96 or total squared residuals greater than 0.25, as poor fits usually indicate proximity to the critical reflectance. If the modeled TOA reflectance was not a monotonic function of $\tau_{0.55}$, AOD retrieval was not attempted. AOD retrieval was also not attempted for bright surfaces with 0.66 μm surface reflectance greater than 0.25, as these surfaces were usually near the critical reflectance. AOD retrieval values were capped at 10 to avoid extrapolation effects on an asymptotic surface.

AOD was corrected for elevation using the simple adjustment applied in the MODIS Collection 4 processing. The Rayleigh optical depth was modified using an exponential profile of the Earth's atmosphere to account for differences at high elevations, since the RTM calculations assume a surface at sea level.

We applied a skewed mean smoothing to the raw 500 m AOD product to generate the final AOD product with an effective resolution of 2.5 km. At each 500 m pixel, we computed a trimmed mean of a 5 × 5 pixel averaging box (up to 25 AOD values) surrounding the center pixel, assigned the result to that center pixel, and added an offset of 0.15 to the resulting value. The 0.15 offset value was an empirically determined value used to reduce the number of negative pixels from the raw AOD output; we suspect that this correction was necessary to adjust for the surface $PM_{2.5}$ in the Central Valley on "clean" summer days (24 h average $PM_{2.5}$ of 10–15 $\mu g/m^3$ for summer 2009) influencing our surface $\xi_{0.66}$ values. The trimmed mean was computed by screening out the top 36% and bottom 12% of AOD values in the averaging box. These screening criteria were identified as the best for this study after performing several comparisons of trimmed and normal means obtained for 1 × 1, 3 × 3, 5 × 5, and 7 × 7 resolutions. The skewed means reduced the number of high AOD outliers that badly impact the relationship between AOD and PM. A 5 × 5 averaging box was chosen as it was the smallest sample that produced stable statistical results. The highest possible spatial resolution was desirable to examine intraurban variability. This smoothing filters out almost half of the data from the AOD analysis, yet retains a higher fraction of raw data than in the operational MODIS land AOD algorithm, which discards at least 70% of the raw reflectance data prior to the 10 × 10 km AOD inversion.

2.6. AOD Validation and $PM_{2.5}$ Predictions

AOD values from both our high-resolution product and the standard Collection 5 AOD algorithm product were compared to AERONET sun photometer measurements obtained during June and July 2008. Data from three coastal AERONET sites in central and northern California—Trinidad Head, Monterey, and UCSB (University of California, Santa Barbara)—were available for comparison. The average of the Terra and Aqua AOD values corresponding to AERONET locations was compared to daily average AERONET AOT values for each available day during the study period; results are shown in Figure 4. The high-resolution AOD product has an R^2 of 0.53 and a slope of 0.63; the standard AOD product has an R^2 of 0.08 and a slope of 0.27. By both measures in this limited data set, the high-resolution AOD is better at matching observed AOT. Additional comparisons of the high resolution and standard AOD product at all PM measurement sites are shown in the supporting information Figure S2. The average of the Terra and Aqua AOD values for individual 2.5 km pixels corresponding to surface measurement locations was compared to $PM_{2.5}$ concentrations averaged from 10:00 A.M. to 2:00 P.M. LST (local standard time), corresponding to the typical satellite overpass times. Linear regression models were created in two ways: day specific and site specific.

In the day-specific model, each day's average 10:00 A.M. to 2:00 P.M. $PM_{2.5}$ surface observations was regressed against the Terra and Aqua average AOD value for all sites within the domain to produce day-specific $PM_{2.5}$–AOD relationships. Daily regressions where the coefficient of determination (R^2) values was below 0.35 were replaced with the bulk fit regression slope of 0.015 AOD/μg/m^3.

For the site-specific method, regression models were run for AOD against 10:00 A.M.to 2:00 P.M. $PM_{2.5}$ surface concentrations for each individual monitoring site across the June 24 to July 31 period to produce site-specific $PM_{2.5}$–AOD relationships. For both methods, intercepts were forced through zero to avoid giving undue influence to high AOD values where surface $PM_{2.5}$ concentrations were low. Outlier observations, defined as being at least three standard deviations from the mean, were removed, and ordinary least squares regression was run on the "outlier-free" data to generate $PM_{2.5}$-AOD relationships. AOD values below zero were set to a $PM_{2.5}$ value of zero, while predicted $PM_{2.5}$ concentrations were capped at 300 μg/m^3, corresponding with the highest observed midday average surface $PM_{2.5}$ concentration during the 2008 fires. No data were withheld because of the need to maximize sample size for regression.

Finally, AOD-predicted $PM_{2.5}$ values were regressed against surface $PM_{2.5}$ concentrations to determine the goodness of fit. Ordinary least squares regression was used, no outliers were removed, and nonzero intercepts were allowed.

3. Results

Figure 5 shows a representative panel plot comparing the visual images of the smoke event, the operational MOD04 Collection 5 AOD product, and our high-resolution AOD product on (top) 27 June 2008 and (bottom) 10 July 2008. Both AOD products are displayed on the same scale. AOD predictions from this work were much more highly

resolved than predictions from the operational AOD algorithm, and this higher resolution allows identifying fine-scale aerosol exposure differences that occur during events that impact urban areas. For example, on 27 June 2008, predicted AOD values differed widely over the Sacramento metropolitan area, yielding AOD values from 1.5 to over 5 in the high-resolution product while the standard operational product smoothed these values. The standard algorithm cloud mask routinely screened out the areas of thickest smoke, especially obvious in the 10 July 2008, image. Note that the high-resolution product did include AOD values in the 27 June 2008 image that is impacted by clouds along the coast and east of the Sierra Nevada Mountains due to the relaxed cloud screen criteria; this product also displays significantly more negative AOD values along the Sierra Nevada Mountains. Moreover, the bright rim of the Central Valley shows a higher AOD, particularly noticeable in the Aqua image near Modesto on 27 June 2008. More accurate characterization of the surface reflectance values along these areas would be expected to reduce the bias associated with the bright surface.

A scatterplot of $PM_{2.5}$ surface concentrations from sites between 36.5° and 41° latitude compared to average daily AOD values is shown in Figure 6. Multiple monitoring sites vulnerable to erroneously high AOD values were excluded from this comparison, including four sites near the ocean or bay in the San Francisco Bay Area, a site in a deep canyon in Yosemite Valley, a site in the eastern Sierra Nevada Mountains near Owens Lake, a site within 500 m of Lake Almanor, and a single site in the Central Valley in Tracy, California. For sites near the lakes, ocean, and bay, sun glint off the water and occasional coastal fog events that were not cloud masked resulted in spuriously high AOD values. The Yosemite site is in a narrow valley surrounded by high granite walls; AOD values returned at this site were routinely negative. Finally, the Tracy, California site is on the dry and bright rim of the Central Valley. The brightness of this surface resulted in spuriously high AOD values.

The main population centers in northern and central California are Sacramento (metropolitan population of 2.7 million), the San Francisco Bay Area (metropolitan population of 7.5 million, including San Jose), and Fresno (metropolitan population of 0.9 million). Comparing across all hourly monitoring $PM_{2.5}$ stations from June 23 to July 31, the highest average observed surface concentrations (55 $\mu g/m^3$) were measured at Chico (population 87,000) in the northeastern portion of the Central Valley. The second highest average $PM_{2.5}$ concentrations (49 $\mu g/m^3$) were measured at Willows (population approximately 6000) on the northwestern edge of the Central Valley. Multiple sites cover the Sacramento area, but Sacramento del Paso is the most centrally located; average $PM_{2.5}$ concentrations at this site were 35 $\mu g/m^3$, and concentrations at other Sacramento area sites were similar or lower during this period. Concentrations in the metropolitan San Francisco Bay Area were much lower, with average concentrations at sites in Berkeley and San Jose averaging 18 and 17 $\mu g/m^3$, respectively, during this period.

While the bulk of the surface $PM_{2.5}$ and AOD data fall below 50 $\mu g/m^3$ and an AOD of 0.75, there is a strong structure of high AOD and $PM_{2.5}$ values well above 100 $\mu g/m^3$, though the high AOD values do not always correspond with high $PM_{2.5}$ and vice versa. This variability is highly dependent on day-specific overpass and $PM_{2.5}$ values and can be explained by a

few specific physical phenomena associated with the California wildfires and topography, described in the discussion section.

A summary of regression fits using the day-specific model for all days is shown in Table 2. Slope values were highly variable from day to day. Of the 38 days, 9 days had R^2 values greater than 0.5. Of the days where R^2 values were less than 0.3, only 5 days had more than three sites where $PM_{2.5}$ concentrations were above 50 μg/m^3. In other words, when surface concentrations were not being affected by smoke from the fires, our method had no predictive power, as expected. Limiting the examination to the 18 days where at least three sites had midday average $PM_{2.5}$ concentrations above 50 μg/m^3, five had R^2 values below 0.2, four had R^2 values between 0.2 and 0.5, and the remaining nine were all above 0.5. In other words, this method showed reasonable predictive capability for surface concentrations on approximately half of the days when smoke impacts were greatest. These results are relatively insensitive to the choice of aerosol optical model; California Typical optical model regressions gave very similar daily R^2, slope, and intercept values. For comparison, day-specific regressions were also calculated using MOD04 Collection 5 AOD. The R^2 values for the MOD04-based regressions are also shown on Table 2. Table 3 provides a summary comparison of average R^2 values segregated by the number of surface sites exhibiting high $PM_{2.5}$ values and therefore likely smoke impact. Neither AOD product is predictive on days with little smoke impact. As smoke impacts become more widespread, the AOD developed here exhibits higher R^2 values. As aerosol load increases, surface characterization becomes less important in the AOD retrieval. The key differences that remain between the two methods during heavy smoke are the spatial resolution, aerosol optical properties, and the cloud mask.

Results of the site-specific regression model are shown in Table 4. Regression statistics at the site level have R^2 values that range from 0.17 to 0.79 and average 0.46 with 11 July included, and range from 0.17 to 0.82 and average 0.60 with 11 July excluded. The temporal regressions done on a site-specific basis have R^2 values that are far higher and more consistent than the spatial regressions done on a day-specific basis.

Figure 7 shows time series of $PM_{2.5}$ surface concentrations and midday average $PM_{2.5}$ predicted concentrations based on our high-resolution AOD product for four surface sites in Chico, Willows, downtown Sacramento, and downtown San Jose. Concentrations at the northernmost sites (Chico and Willows) were highly variable, with concentrations changing by over 100 μg/m^3 within a few hours when major smoke plumes impacted the sites. Overall, the AOD-predicted $PM_{2.5}$ concentrations track the midday concentrations relatively well at all of these sites, although there were multiple days when surface $PM_{2.5}$ concentrations were significantly overpredicted. For example, concentrations were slightly overpredicted at several sites in 25 June and greatly overpredicted at several sites in 8 and 11 July (Figure 7). Inspection of visual images reveals thick plumes of smoke over most of the Central Valley on each of these days; the AOD predictions of surface $PM_{2.5}$ are too high for some other reason. It is likely that vertical stratification of smoke from the high-elevation fires led to high column AOD that does not represent surface conditions. Buoyant smoke plumes emitted from high-elevation areas in the mountains may not mix down to the valley floor when winds are highest during frontal passages. Overall, though,

it is clear that the general shape of the episodes is captured well by this method and that predicted concentrations on many of the days of the episode are likely be representative of true exposures experienced during the events.

Given the general success of the method in reproducing general time series of midday $PM_{2.5}$ concentrations at available surface monitoring sites during fire episode days when concentrations were elevated, we present a close-up of predicted $PM_{2.5}$ concentrations for some of the key episode days in the Sacramento Valley when concentrations and potential exposures were highest. The panel plots in Figure 8 display the predicted $PM_{2.5}$ concentrations in 24 and 27 June, 9 and 10 July, and 23–26 July. These images demonstrate both the large $PM_{2.5}$ impacts in the region and the spatial variability evident in the high-resolution product.

4. Discussion

Previous attempts to predict surface $PM_{2.5}$ concentrations over the western United States have found that MODIS AOD has poor correlation with 24 h average surface PM [Engel-Cox et al., 2004a, 2004b; Green et al., 2009; Hu, 2009]. Hu [2009] found that no sites in California had an annual average correlation coefficient greater than ~0.4; most monitors had regression coefficients between 0.1 and 0.2. Improved correlations of MODIS AOD with AERONET AOD measurements were shown by Drury et al. [2008] and Castanho et al. [2007] over the western United States and Mexico City, respectively, when surface reflectance ratios were improved. However, neither of these studies attempted to directly infer surface $PM_{2.5}$ concentrations with their methods. Improvements to western U.S. surface PM predictions have been seen with the addition of Multiangle Imaging Spectroradiometer (MISR) multispectral AOD retrievals to account for particulate matter component optical properties, such as NO_3 [Liu et al., 2007; van Donkelaar et al., 2010]. However, MISR observes any given section of our domain only about once every 9 days, yielding insufficient coverage during fire events to be useful for this purpose.

Additionally, a few previous studies have explored the possibility of providing a high-resolution AOD product [Castanho et al., 2007, 2008; Li et al., 2005]. Castanho's 2007 study demonstrated the possibility of using the technique over Mexico City and demonstrated high correlations between 1.5 × 1.5 km AOD and sun photometers when surface reflectance ratios were corrected. Similarly, Li et al. [2005] demonstrated a 1 × 1 km MODIS AOD product and found that their product had predictive power for surface PM_{10} measurements over 3 days (September 15–17) with R values of 0.86, 0.55, and 0.68, which correspond to R^2 values of 0.70, 0.30, and 0.46, respectively.

Multiple factors were found to influence the final results. Of these, the ones that were found to have the most importance in terms of predicting $PM_{2.5}$ concentrations at the surface included the vertical stratification of smoke, temporal variability in $PM_{2.5}$ concentrations, surface reflectance ratio values, and differences in mixing heights within the study domain. The vertical stratification of smoke layers above the planetary boundary layer is the most important factor influencing individual day results for predicting $PM_{2.5}$ concentrations. California's Central Valley is a large basin with elevations ranging from a few meters above

sea level to 80 m above sea level. In contrast, elevations in the Sierra Nevada Mountains east of the valley are between 1500 and 2700 m and the North Coast mountain ranges west of the valley are typically above 300 m. Fires in both mountain ranges burned at elevations hundreds to thousands of meters above the valley floor. Buoyant smoke plumes from active fires can be lofted above the planetary boundary layer [e.g., Kahn et al., 2007,2008]. Val Martin et al. [2010] found that between 4% and 12% of the smoke plumes from the California fires were injected above the boundary layer, with the greatest heights occurring in June–July. Further, they found a positive relationship between plume heights and fire intensity, as measured by MODIS total fire radiative power. Given the combination of high elevations and intense fires, it is likely that some of the smoke from the fires was lofted above the Central Valley's boundary layer or did not completely mix to the surface. Multiple observations of low $PM_{2.5}$ concentrations at the surface and high AOD values produce poor correlations between surface $PM_{2.5}$ and AOD on individual days. We believe that results for 26 June, 8 July, 11 July, and 22 July show significant evidence of at least five sites where AOD values were high and surface $PM_{2.5}$ concentrations were very low on both absolute and percentage bases. Each of these days also corresponds with a major frontal passage initiating or ending an episode of higher smoke concentrations. The high winds on these days may have caused incomplete mixing to the surface. Moreover, dense smoke can prevent radiative heating of the surface, thus leading to a more stable planetary boundary layer, lower mixing heights, and a further induction of vertical stratification of smoke from buoyant plumes [Stone et al., 2008].

Aerosol backscatter data from the Cloud-Aerosol Lidar and Infrared Pathfinder Satellite Observation (CALIPSO) satellite can provide information on the vertical profile of smoke plumes when the satellite passes directly over the plume. Unfortunately, the narrow CALIPSO footprint precludes assessment on most days during the event. An overpass in 9 July did pass through the domain. Figure 9 is the browse image of the 532 nm channel total attenuated backscatter from the Cloud-Aerosol Lidar with Orthogonal Polarization (CALIOP) instrument on board CALIPSO. This transect suggests that aerosol near the fires in the Sierra Nevada Mountains was injected to 5 km but was well mixed within the boundary layer by the time it reached the Sacramento Valley to the south. The gap in observed backscatter between the surface and the main plume at higher elevations may be evidence of decoupling between AOD and surface $PM_{2.5}$, as suggested by the low $PM_{2.5}$ concentrations at the Chico site that day, but the gap may also be due to signal saturation.

Another factor that makes the prediction of $PM_{2.5}$ surface concentrations complicated is the large variation in observed concentrations when plumes impact monitoring sites. Concentrations in the 5 h overpass window (10:00 A.M. to 2:00 P.M. LST) had standard deviations greater than 20 $\mu g/m^3$ in approximately one out of every seven occurrences when the overpass mean was greater than 15 $\mu g/m^3$. Some of this structure can be seen in the time series of $PM_{2.5}$ concentrations in Figure 6. Similarly, the coefficient of variance (standard deviation divided by the mean) exceeded 0.4 more than 1 out of 6 times for the same subset of data. When 15% of the $PM_{2.5}$ measurements have highly variable concentrations within a 5 h window due to the effects of local smoke plumes, it is much more difficult to predict the domain average concentrations accurately with an average of two overpass snapshots of the local conditions.

The accurate characterization of surface reflectance ratio values was problematic for some of the monitoring sites within the study domain. Our method used surface reflectance ratio values from 2009 to estimate what the values were during the 2008 fire season. We could not use 2008 because of the influence of the smoke and because California's Central Valley spectral signature can change rapidly from green to brown during the summer dry season. A comparison of Central Valley temperature and precipitation patterns for 2009 and 2008 indicated that 2009 patterns were generally similar, although slightly wetter in the spring. This may have resulted in underprediction of surface reflectance ratios for 2008, especially in areas free of irrigation or human landscaping (such as the brown ring around the valley seen in Figure 5). Sites along this ring would be most affected, and information from one site (Tracy) was so consistently poor that it was not used for the regression analysis. This surface reflectance ratio issue has been seen in the western United States and in urban areas in previous work [Castanho et al., 2007; Engel-Cox et al., 2004a, 2004b; Oo et al., 2010]. Errors in estimating surface reflectance ratios across the monitoring sites in the domain will result in more variable day-specific regression uncertainty, whereas the site-specific regressions will be systematically biased in a way that can be accounted for in the regression statistics.

Another potentially important issue with the method is differences in mixing heights within the study domain on individual days. Previous work has shown that mixing heights during the summer ozone season can vary dramatically across the Central Valley. During an ozone episode in early August 1990, mixing heights were determined to change by more than a factor of three within the valley, ranging from approximately 300 to 1200 m in height during the same day in different parts of the valley [Blumenthal et al., 1997]. Differences in mixing heights across the valley may be sufficient to introduce significant differences in predicted concentrations on individual episode days during a fire event. Also, these intravalley differences may be exacerbated by the smoke-albedo feedback, leading to even larger differences in mixing heights between the smoke-covered areas and those portions of the valley with less dense smoke. Thus, the goal of capturing differences in mixing heights that affect AOD-$PM_{2.5}$ relationships on a daily basis may be somewhat confounded by the differences in mixing heights exhibited within the Central Valley.

Using an air quality model to help tie mixing height and aerosol properties to satellite data is a promising method for capturing daily differences [van Donkelaar et al., 2011]. However, the complex topography and meteorology would complicate model evaluation at the surface sites closest to the fires (e.g., Chico). Additionally, the resolution of the air quality model would need to be at a comparable spatial scale to the high-resolution AOD product created in this exercise. To our knowledge, no attempts have been made to link high-resolution satellite AOD products with high-resolution air quality model output.

5. Conclusions

We estimated midday surface-level $PM_{2.5}$ concentrations during the 2008 Northern and Central California wildfires using a high-resolution MODIS AOD product. On days when $PM_{2.5}$ concentrations were high and smoke was well mixed vertically, the high-resolution AOD product routinely captured more than 50% of the variance in surface $PM_{2.5}$

concentrations. On days with widespread smoke observed at ground-based monitors, the high-resolution AOD product was better correlated to $PM_{2.5}$ than MOD04 Collection 5. However, it was also determined that spatial and vertical variability in $PM_{2.5}$ concentrations from the smoke events resulted in very poor predictions of surface $PM_{2.5}$ on some days. The temporal correlation of AOD and outlier-free $PM_{2.5}$ at 26 sites showed strong relationships (mean R^2= 0.60, 0.17 ≤R^2 ≤ 0.82). On days when basic assumptions regarding vertical mixing of smoke are met, the high-resolution AOD product can be used to predict midday $PM_{2.5}$ concentrations in cities at an effective resolution of 2.5 km, yielding useful information for epidemiological exposure studies for fire events. The three significant scientific advancements in this work are the ability to make $PM_{2.5}$ concentration estimates from MODIS satellite data (1) with high-spatial resolution (2.5 km), (2) during wildfires, and (3) in areas with bright land surfaces (e.g., the western United States). Because the general population may receive their highest PM exposures of any given year during wildfire events, the development represents a significant improvement in characterizing exposure more accurately.

Supplementary Material

Refer to Web version on PubMed Central for supplementary material.

Acknowledgments.

The authors would like to thank Andrea de Castanho for her invaluable early guidance and support and the National Institute of Environmental Health Science for funding under grant 1R21ES016986-02. We also thank the AERONET site principal investigators Brent Holben, Ellsworth Dutton, and Jeffrey Reid for their efforts in establishing and maintaining the UCSB, Trinidad Head, and Monterey sites.

References

Bhartia PK, McPeters RD, Mateer CL, Flynn LE, and Wellemeyer C (1996), Algorithm for the estimation of vertical ozone profiles from the backscattered ultraviolet technique, J. Geophys. Res, 101, 18,793–18,806, doi:10.1029/96JD01165.

Blumenthal DL, Lurmann FW, Roberts PT, Main HH, MacDonald CP, Knuth WR, and Niccum EM (1997), Three-dimensional distribution and transport analyses for SJVAQS/AUSPEX. Final report prepared for the San Joaquin Valley Air Pollution Study Agency, Sacramento, CA, by Sonoma Technology, Inc., Santa Rosa, CA, Technical & Business Systems, Santa Rosa, CA, and California Air Resources Board, Sacramento, CA, STI-91060-1705-FR, February.

California Air Resources Board (2012), 2008 Northern California Wildfires. Web page at http://www.arb.ca.gov/desig/excevents/2008wildfires.htm. January 17.

Castanho ADA, Prinn R, Martins V, Herold M, Ichoku C, and Molina LT (2007), Analysis of Visible/SWIR surface reflectance ratios for aerosol retrievals from satellite in Mexico City urban area, Atmos. Chem. Phys, 7, 5467–5477.

Castanho ADA, Martins JV, and Artaxo P (2008), MODIS aerosol optical depth retrievals with high spatial resolution over an urban area using the critical reflectance. J. Geophys. Res 113, D02201, doi:10.1029/2007JD008751.

Delfino RJ, et al. (2009), The relationship of respiratory and cardiovascular hospital admissions to the southern California wildfires of 2003, Occup. Environ. Med, 66(3), 189–197, March. [PubMed: 19017694]

Derber J, Parrish D, and Lord SJ (1991), The new global operational analysis system at the National Meteorological Center, Weather Forecasting, 6, 538–547.

Drury E, Jacob DJ, Wang J, Spurr RJD, and Chance K (2008), Improved algorithm for MODIS satellite retrievals of aerosol optical depths over western North America, J. Geophys. Res, 113, D16204, doi:10.1029/2007JD009573.

Dubovik O, and King MD (2000), A flexible inversion algorithm for retrieval of aerosol optical properties from Sun and sky radiance measurements, J. Geophys. Res, 105(D16), 20,673–20,696, August 27.

Engel-Cox J, Hoff R, and Haymet A (2004a), Recommendations on the use of satellite remote-sensing data for urban air quality, J. Air Waste Manage, 54, 1360–1371.

Engel-Cox JA, Holloman CH, Coutant BW, and Hoff RM (2004b), Qualitative and quantitative evaluation of MODIS satellite sensor data for regional and urban scale air quality, Atmos. Environ, 38(16), 2495–2509.

Fraser R, and Kaufman YJ (1985), The relative importance of aerosol scattering and absorption in remote sensing, IEEE Trans. Geosci. Remote Sens, GE-23(5), 625–633.

Green M, Kondragunta S, Ciren P, and Xu C (2009), Comparison of GOES and MODIS aerosol optical depth (AOD) to aerosol robotic network (AERONET) AOD and IMPROVE $PM_{2.5}$ mass at Bondville, Illinois, J. Air Waste Manage, 59(9), 1082–1091, doi:10.3155/1047-3289.59.9.1082.

Gupta P, Christopher SA, Wang J, Gehrig R, Lee YC, and Kumar N (2006), Satellite remote sensing of particulate matter and air quality assessment over global cities, Atmos. Environ, 40, 5880–5892.

Holben BN, et al. (1998), AERONET–A federated instrument network and data archive for aerosol characterization, Remote Sens. Environ, 66, 1–16.

Hu Z (2009), Spatial analysis of MODIS aerosol optical depth, $PM_{2.5}$, and chronic coronary heart disease, Int. J. Health Geographics, 8(27), doi:10.1186/1476-072X-8-27.

Kahn RA, Li W-H, Moroney C, Diner DJ, Martonchik JV, and Fishbein E (2007), Aerosol source plume physical characteristics from space-based multiangle imaging. J. Geophys. Res, 112, D11205, 1–20, doi:10.1029/2006JD007647.

Kahn RA, Chen Y, Nelson DL, Leung F-Y, Li Q, Diner DJ, and Logan JA (2008), Wildfire smoke injection heights: Two perspectives from space, Geophys. Res. Lett, 35, L04809, doi:10.1029/2007GL032165.

Kaufman YJ (1987), Satellite sensing of aerosol absorption, J. Geophys. Res, 92(D4), 4,307–4,317, doi:10.1029/JD092iD04p04307.

Kaufman YJ, and Fraser RS (1997), The effect of smoke particles on clouds and climate forcing, Science, 277(5332), 1636–1639, doi:10.1126/science.277.5332.1636, September.

Kaufman Y, Tanré D, and Boucher O (2002), A satellite view of aerosols in the climate system, Nature, 419, 215–223. [PubMed: 12226676]

Kotchenova SY, and Vermote EF (2007), Validation of a vector version of the 6S radiative transfer code for atmospheric correction of satellite data. Part II: Homogeneous Lambertian and anisotropic surfaces, Appl. Opt, 46(20), 4455–4464. [PubMed: 17579701]

Kotchenova SY, Vermote EF, Matarrese R, and Klemm FJ (2006), Validation of a vector version of the 6S radiative transfer code for atmospheric correction of satellite data. Part 1: Path radiance, Appl. Opt, 45(26), 6762–6774. [PubMed: 16926910]

Künzli N, et al. (2006), Health effects of the 2003 Southern California wildfire on children, Am. J. Respir. Crit. Care Med, 174, 1221–1228. [PubMed: 16946126]

Li C, Lau AK-H, Mao J, and Chu DA (2005), Retrieval, validation, and application of the 1-km aerosol optical depth from MODIS measurements over Hong Kong, IEEE Trans. Geosci Remote Sens, 43(11), 2650–2658, doi:10.1109/TGRS.2005.856627.

Liu Y (2004), Variability of wildland fire emissions across the contiguous United States, Atmos. Environ, 38, 3489–3499, doi:10.1016/j.atmosenv.2004.02.004.

Liu Y, Franklin M, Kahn R, and Koutrakis P (2007), Using aerosol optical thickness to predict ground-level $PM_{2.5}$ concentrations in the St. Louis area: A comparison between MISR and MODIS, Remote Sens. Environ, 107, 33–44.

Martins JV, Artaxo P, Liousse C, Reid JS, Hobbs PV, and Kaufman YJ (1998), Effects of black carbon content, particle size, and mixing on light absorption by aerosols from biomass burning in Brazil, J. Geophys. Res, 103(D24), 32,041–32,050, doi:10.1029/98JD02593.

Naeher LP, Brauer M, Lipsett M, Zelikoff JT, Simpson CD, Koenig JQ, and Smith KR (2007), Woodsmoke health effects: A review, Inhalation Toxicol., 19, 67–106, doi:10.1080/08958370600985875.

Neuendorffer AC (1996), Ozone monitoring with TIROS-N operational vertical sounders, J. Geophys. Res, 101(D13), 18,807–18,828, doi:10.1029/96JD01063.

Omar AH, Won J-G, Winker DM, Yoon S-C, Dubovik O, and McCormick MP (2005), Development of global aerosol models using cluster analysis of Aerosol Robotic Network (AERONET) measurements, J. Geophys. Res, 110, D10S14, doi:10.1029/2004JD004874.

Oo MM, Jerg M, Hernandez E, Picon A, Gross BM, Moshary F, and Ahmed SA (2010), Improved MODIS aerosol retrieval using modified VIS/SWIR surface albedo ratio over urban scenes, IEEE Trans. Geosci Remote Sens, 48(3), doi:10.1109/TGRS.2009.2028333.

Reid SB, Huang S, Pollard EK, Craig KJ, Sullivan DC, Zahn P, MacDonald C, and Raffuse SM (2009), An almanac for understanding smoke persistence during the 2008 fire season, Final report prepared for the USDA Forest Service, Pacific Southwest Region, by Sonoma Technology, Inc., Petaluma, CA, STI-908045-3747-FR, November 5.

Remer LA, Tanre D, Kaufman YJ, Levy RC, and Matoo S (2009), Algorithm for remote sensing of tropospheric aerosol from MODIS: Collection 005: Revision 2. Algorithm theoretical basis document version 2.0, prepared for the National Aeronautics and Space Administration.

Schreuder AB, Larson TV, Sheppard L, and Claiborn CS (2006), Ambient woodsmoke and associated respiratory emergency department visits in Spokane, Washington, Int. J. Occup. Environ. Health, 12(2), 147–153. [PubMed: 16722195]

Sood A, Petersen H, Blanchette CM, Meek P, Picchi MA, Belinsky SA, and Tesfaigzi Y (2010), Wood smoke exposure and gene promoter methylation are associated with increased risk for COPD in smokers, Am J Respir Crit Care Med, 182, 1098–1104, doi:10.1164/rccm.201002-02220C. [PubMed: 20595226]

Stone RS, Anderson GP, Shettle EP, Andrews E, Loukachine K, Dutton EG, Schaaf C, and Roman MO (2008), Radiative impact of boreal smoke in the Arctic: Observed and modeled, J. Geophys. Res, 113, D14S16, doi:10.1029/2007JD009657.

Val Martin M, Logan JA, Kahn RA, Leung FY, Nelson DL, and Diner DJ (2010), Smoke injection heights from fires in North America: Analysis of 5 years of satellite observations, Atmos. Chem. Phys, 10, 1491–1510.

van Donkelaar A, Martin RV, Brauer M, Kahn R, Levy R, Verduzco C, and Villeneuve PJ (2010), Global estimates of exposure to fine particulate matter concentrations from satellite-based aerosol optical depth: Development and application, Environ. Health Perspect, 118(6), doi:10.1289/ehp.0901623.

van Donkelaar A, Martin RV, Levy RC, da Silva AM, Krzyzanowski M, Chubarova N, Semutnikova E, and Cohen AJ (2011), Satellite-based estimates of ground-level fine particulate matter during extreme events: A case study of the Moscow fires in 2010, Atmos. Environ, 45, doi:10.1016/j.atmosenv.2011.07.068.

Vaughan MA, Young SA, Winker DM, Powell KA, Omar AH, Liu Z, Hu Y, and Hostetler CA (2004), Fully automated analysis of space-based lidar data: An overview of the CALIPSO retrieval algorithms and data products, Proc. SPIE, 5575, 16–30, doi:10.1117/12.572024.

Vermote EF, Tanre D, Deuze JL, Herman M, and Morcrette J-J (1997), Second simulation of the satellite signal in the solar spectrum, 6S: An overview, IEEE Trans. Geosci. Remote Sens, 35(3), doi:10.1109/36.581987.

Vermote EF, El Saleous NZ, and Justice CO (2002), Atmospheric correction of MODIS data in the visible to middle infrared: First results, Remote Sens. Environ, 83, 97–111.

Wu J, Winer A, and Delfino R (2006), Exposure assessment of particulate matter air pollution before, during, and after the 2003 southern California wildfire, Atmos. Environ, 40, 3333–3348.

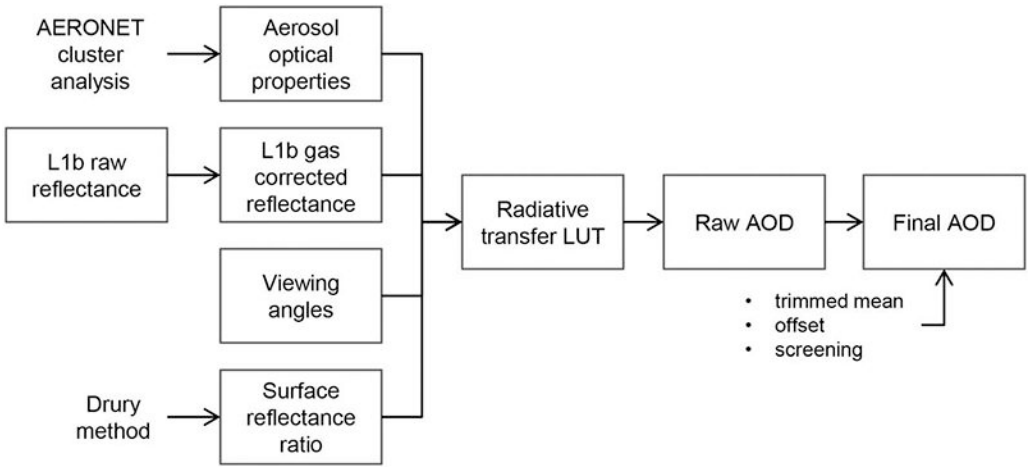

Figure 1.
Schematic of the algorithm components for creating a high-resolution AOD product.

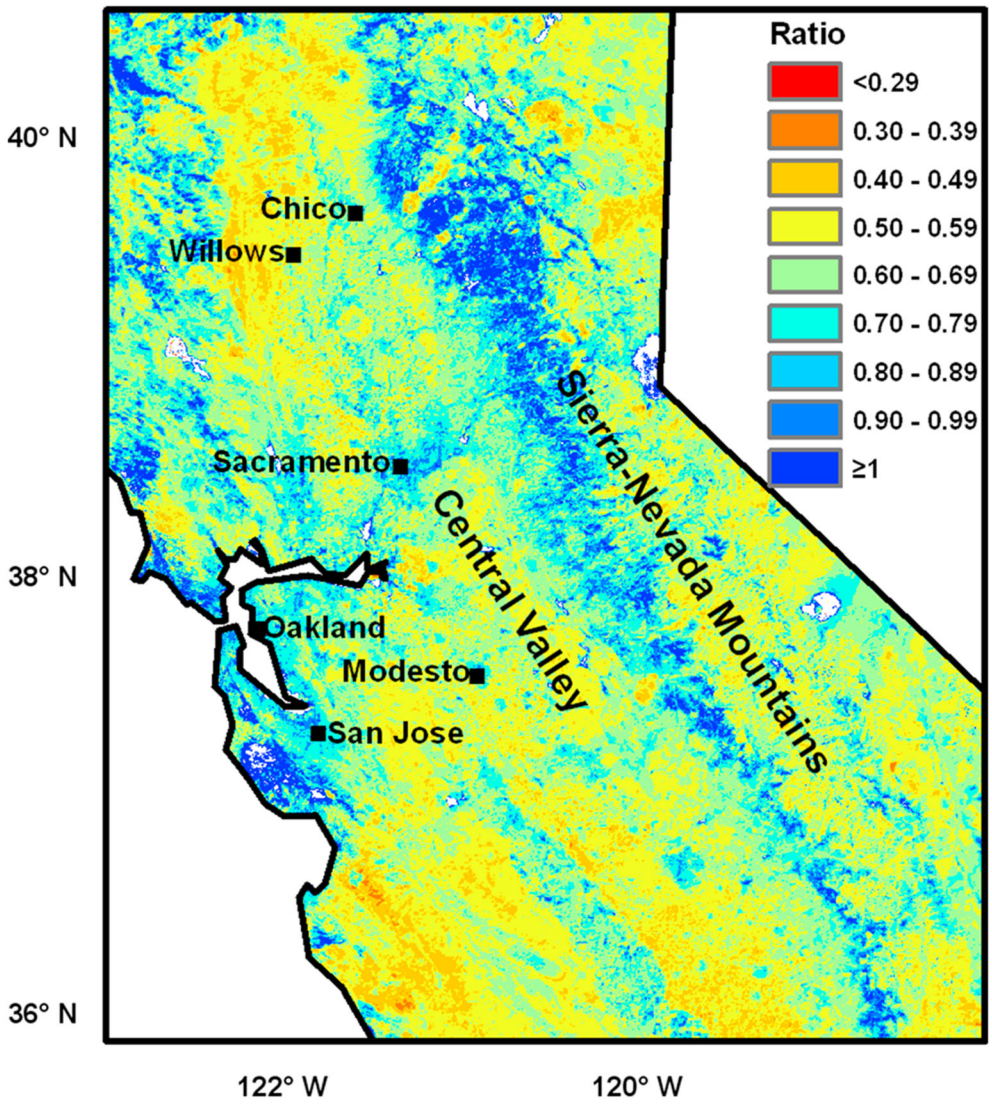

Figure 2.

Average clean day surface reflectance ratios (ξ0.66) calculated using Terra satellite data from June to August 2009.

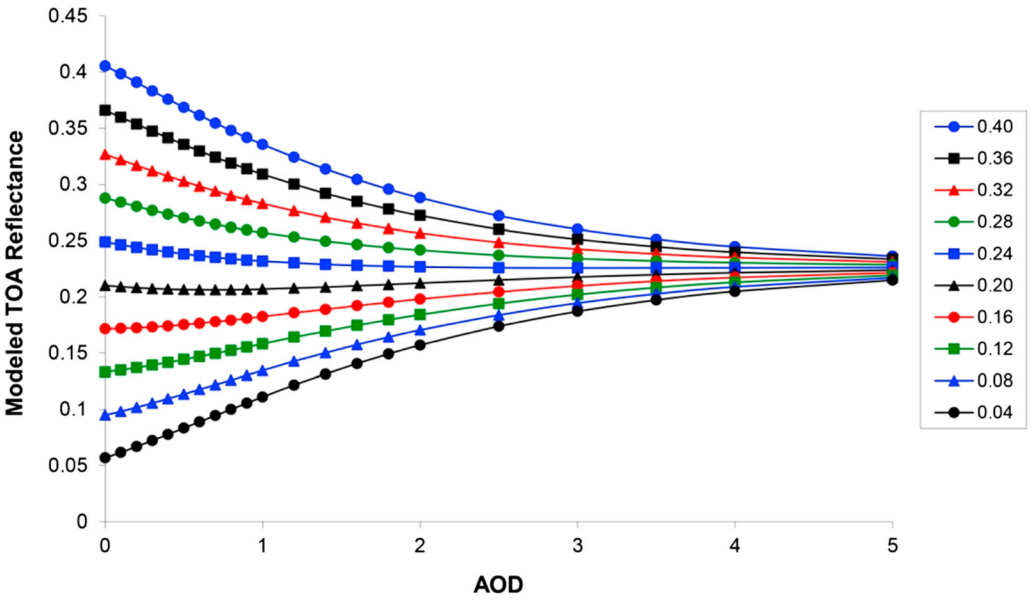

Figure 3.

TOA reflectance at 0.66 μm modeled by the 6S RTM as a function of aerosol optical depth at 0.55 μm for surface reflectances ranging from 0.04 to 0.40 using optical properties of the biomass burning aerosol for solar zenith of 12°, view zenith of 18°, and relative azimuth of 132°.

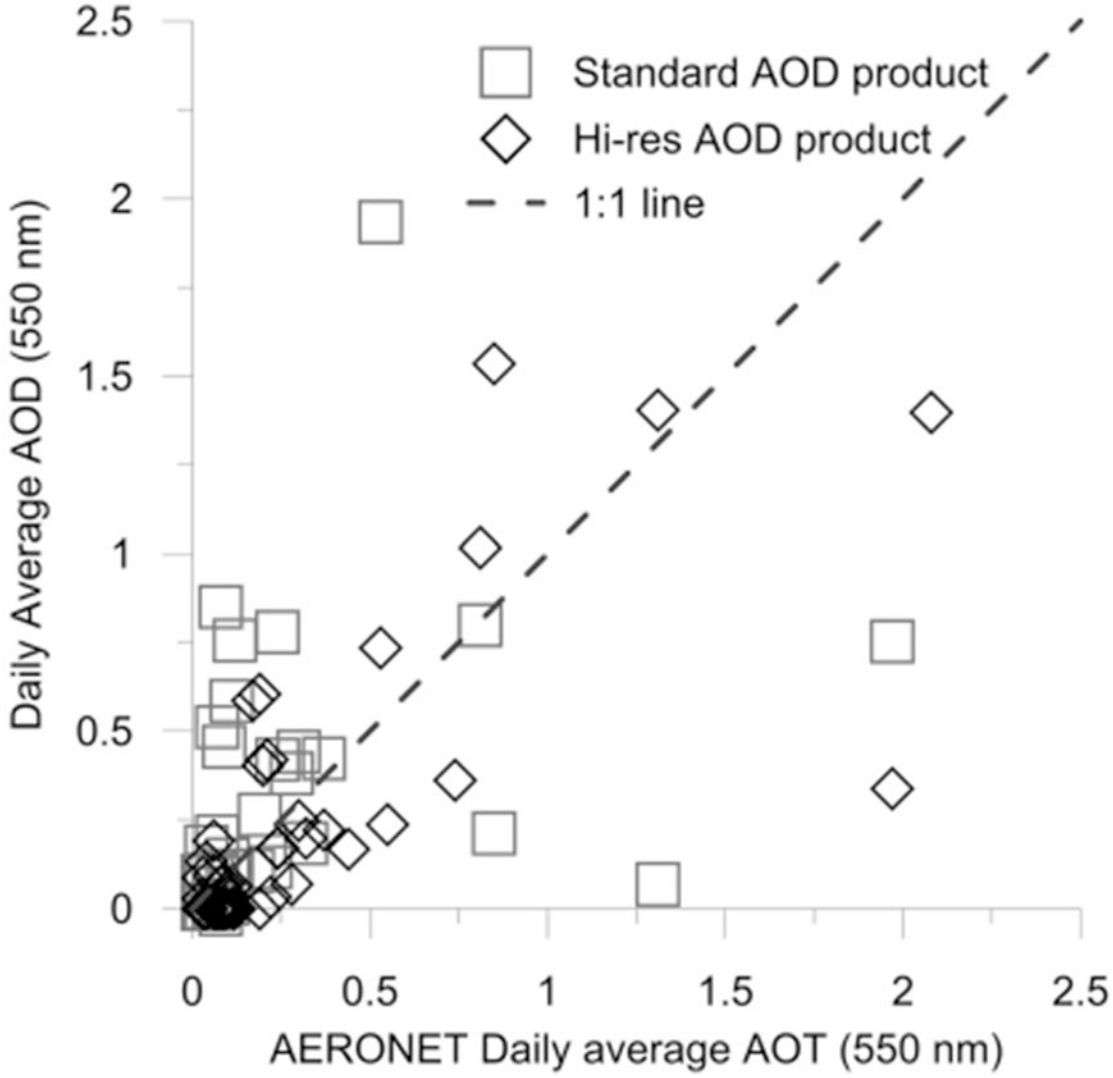

Figure 4.
Comparison of AERONET daily average AOT from the UCSB, Monterey, and Trinidad Head to high-resolution product AOD (open diamonds) and standard MOD04 Collection 5 AOD (open squares). The 1:1 line is also shown.

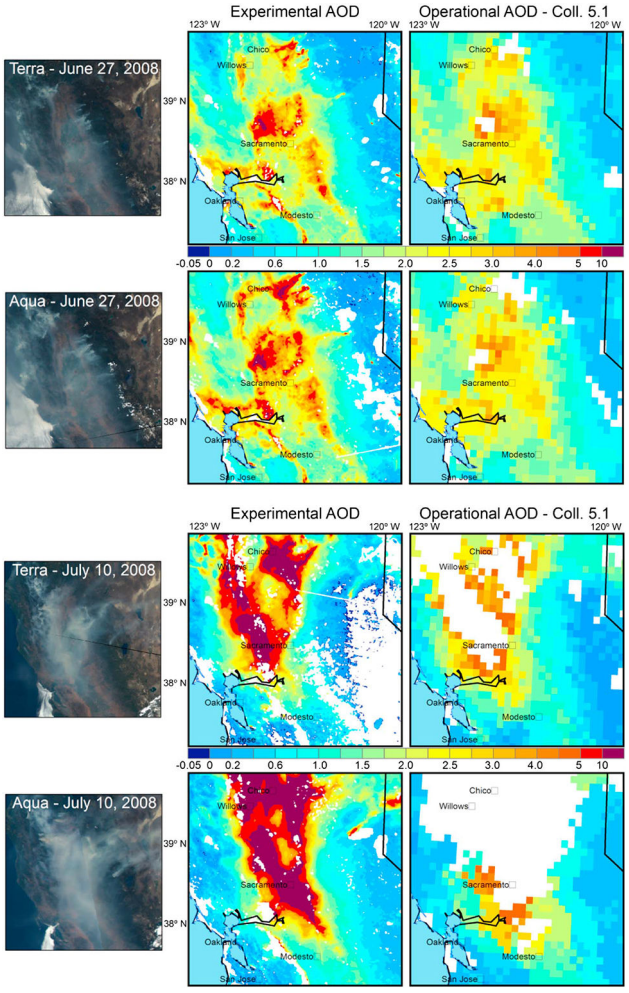

Figure 5.

Comparison of visible images and AOD products from this work (experimental AOD) and the standard operational algorithm (operational AOD) on 27 June 2008 (top) and on 10 July 2008 (bottom).

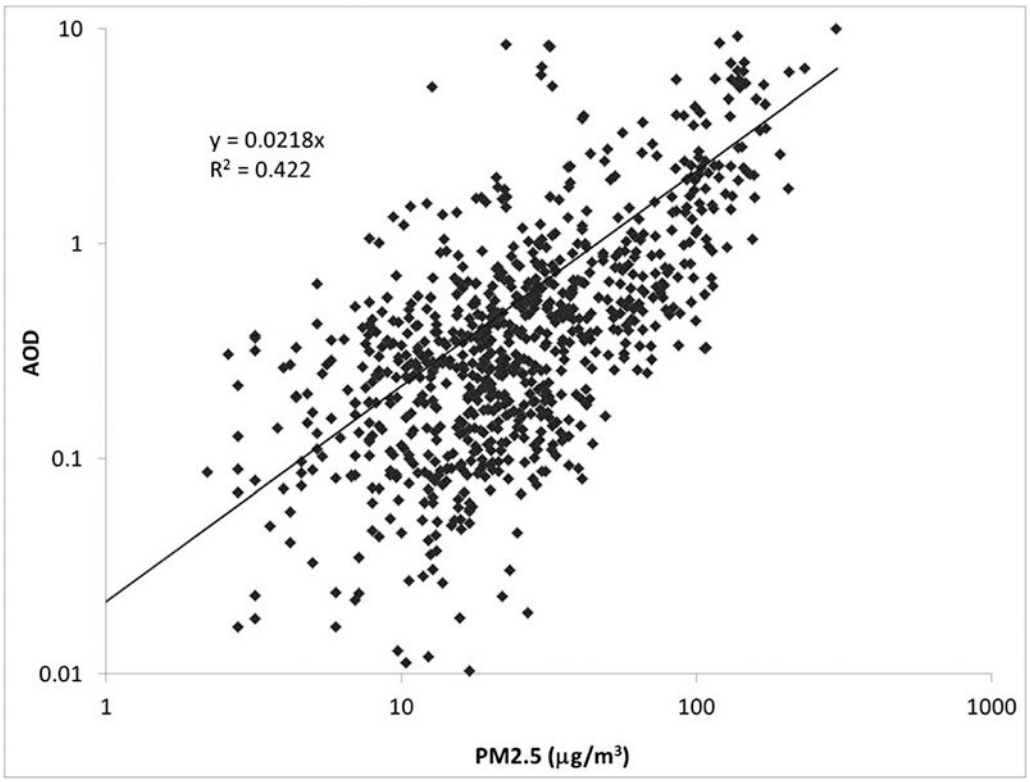

Figure 6.

Comparison of 10:00 A.M. to 2:00 P.M. average $PM_{2.5}$ concentrations ($\mu g/m^3$) with average daily AOD values at surface monitoring sites in central and northern California from 24 June to 31 July 2008.

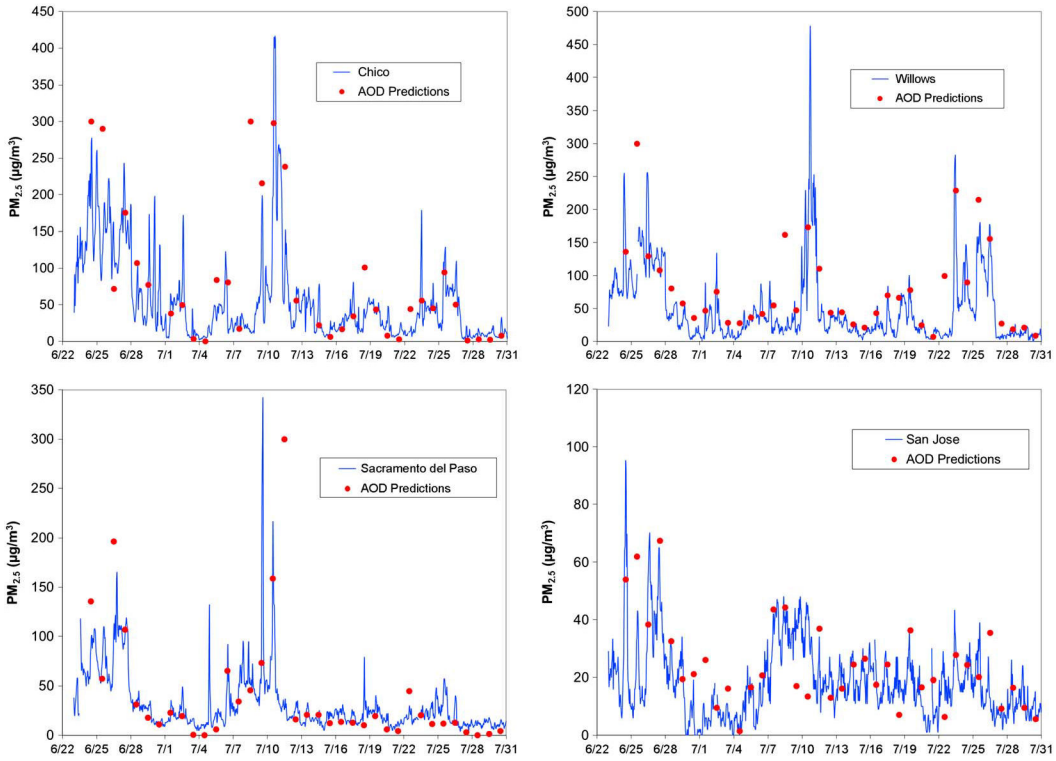

Figure 7.

Time series of surface $PM_{2.5}$ concentrations (µg/m^3)and predicted midday $PM_{2.5}$ concentrations based on kernel-smoothed 5 × 5 pixel comparisons at Chico (top left), Willows (top right), Sacramento del Paso (bottom left), and San Jose (bottom right). Note that the scale of $PM_{2.5}$ concentrations changes for each time series, especially San Jose.

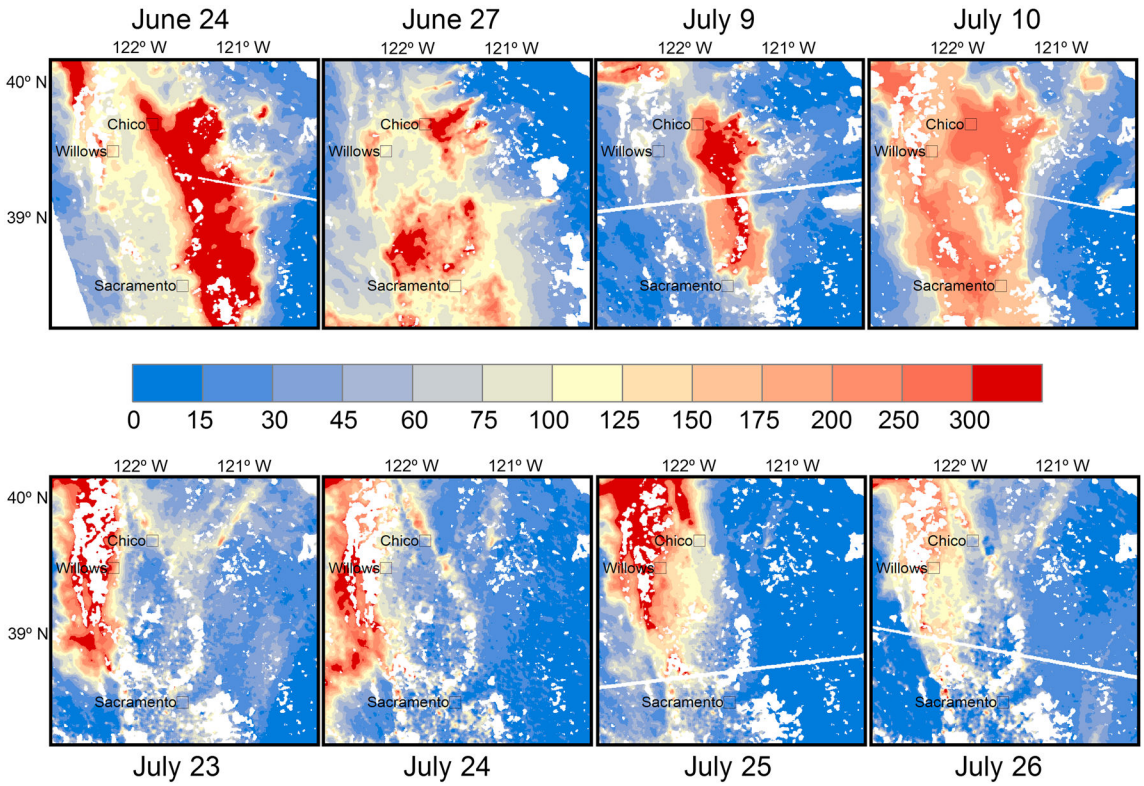

Figure 8.

Maps of predicted $PM_{2.5}$ concentration ($\mu g/m^3$) for key episode days based on Terra and Aqua averaged AOD. Blank pixels indicate that both satellite overpass values were invalidated or cloud screened.

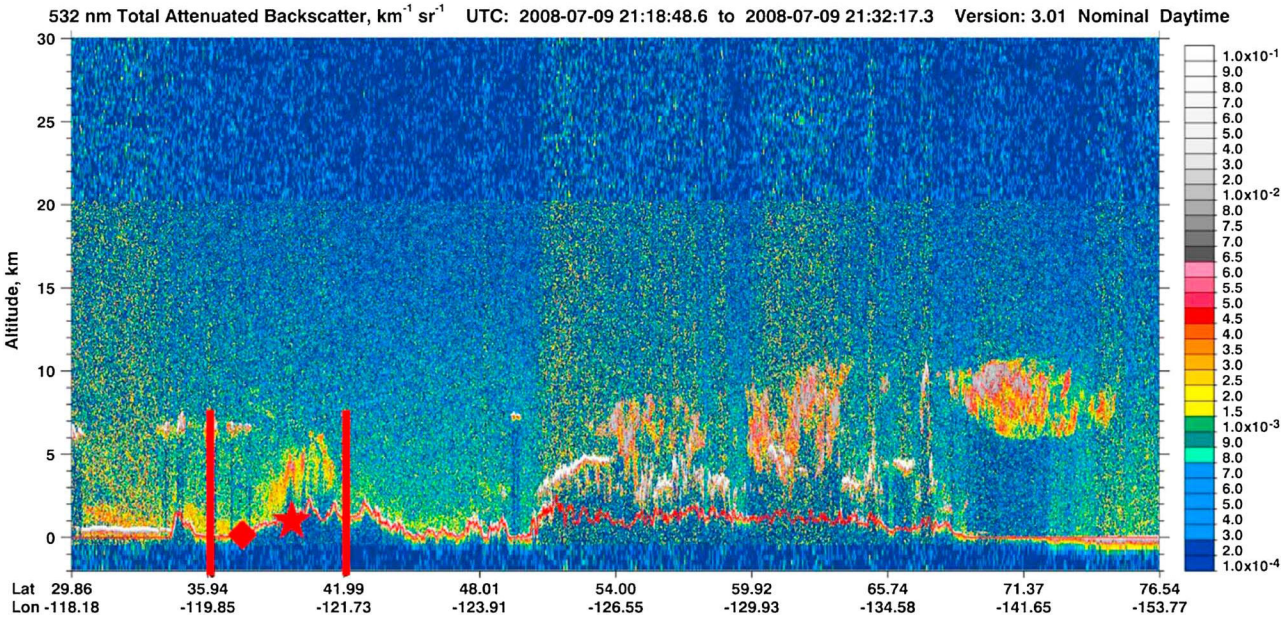

Figure 9.

Annotated browse image of the 532 nm total attenuated backscatter from the CALIPSO satellite overpass on 9 July 2008. The red bars represent the approximate bounds of the study domain. The star and diamond between latitude 35.94 and 41.99 show the locations for Chico and Sacramento, respectively. Image source: Vaughan et al. [2004].

Table 1.

Range of Parameters Used in the Radiative Transfer Model Simulations for the TOA-to-AOD Look-Up Tables

Parameter	Values
Solar zenith angle	0, 12, 24, 36, 48, 54, 60, 66, 72
Sensor zenith angle	0, 6, 12, 18, 24, 30, 36, 42, 48, 54, 60, 66, 72
Relative sun/sensorazimuth angle	0, 12, 24, 36, 48, 60, 72, 84, 96, 108, 120, 132, 144, 156, 168, 180
Surface reflectance	0.002, 0.005, 0.01, 0.02, 0.03, 0.04, 0.05, 0.06, 0.07, 0.08, 0.09, 0.10, 0.11, 0.12, 0.13, 0.14, 0.15, 0.16, 0.18, 0.20, 0.22, 0.24, 0.26, 0.28, 0.30, 0.32, 0.34, 0.36, 0.38, 0.40, 0.42, 0.44
Aerosol optical depth (biomass burning aerosol)	0.0, 0.1, 0.2, 0.3, 0.4, 0.5, 0.6, 0.7, 0.8, 0.9, 1.0, 1.2, 1.4, 1.6, 1.8, 2.0, 2.5, 3.0, 3.5, 4.0, 5.0

Table 2.

Adjusted Regression Statistics for Comparisons of Predicted Surface $PM_{2.5}$ Concentrations to Measured Surface $PM_{2.5}$ Concentrations by Day[a]

Date	R^2	Slope	Slope Error	Constant (μg/m^3)	Constant Error μg/m^3)	Number of Surface Sites > 50 μg/m^3	MOD04 R^2
6/24/2008	0.527	0.32	0.07	61	9	24	0.335
6/25/2008	0.236	0.18	0.07	73	9	22	0.096
6/26/2008	0.133	0.21	0.10	74	15	22	0
6/27/2008	0.536	0.74	0.14	20	15	23	0.328
6/28/2008	0.022	0.17	0.14	30	7	3	0.001
6/29/2008	0.344	0.45	0.13	16	5	1	0.183
6/30/2008	0.072	−0.27	0.17	17	3	1	0
7/1/2008	0.226	0.61	0.22	6	8	3	0.275
7/2/2008	0.07	0.20	0.12	28	8	5	0.465
7/3/2008	0.009	−0.10	0.09	12	2	0	0.069
7/4/2008	0.165	0.21	0.10	7	1	0	0
7/5/2008	0.391	0.42	0.11	14	3	2	0.579
7/6/2008	0.26	0.43	0.14	20	7	8	0.396
7/7/2008	0.346	0.59	0.16	15	8	8	0.466
7/8/2008	0.048	−0.10	0.06	45	6	10	0.064
7/9/2008	0.772	0.65	0.08	30	7	12	0.271
7/10/2008	0.674	0.58	0.09	39	12	17	0.337
7/11/2008	0.018	0.04	0.04	25	7	4	0.083
7/12/2008	0.019	0.15	0.13	20	4	1	0
7/13/2008	0	0.12	0.13	20	3	1	0.406
7/14/2008	0	0.00	0.25	21	7	1	0.075
7/15/2008	0	−0.07	0.11	20	2	0	0.029
7/16/2008	0.013	0.13	0.11	17	3	0	0
7/17/2008	0.14	0.40	0.18	9	5	0	0.237
7/18/2008	0.135	0.23	0.11	19	4	2	0.191
7/19/2008	0.558	0.64	0.12	11	4	3	0.679
7/20/2008	0	0.10	0.22	13	5	0	0

J Geophys Res Atmos. Author manuscript; available in PMC 2022 November 03.

Date	R^2	Slope	Slope Error	Constant ($\mu g/m^3$)	Constant Error $\mu g/m^3$)	Number of Surface Sites > 50 $\mu g/m^3$	MOD04 R^2
7/21/2008	0	−0.09	0.11	11	2	0	0
7/22/2008	0	0.00	0.05	16	2	0	0
7/23/2008	0.74	0.86	0.11	1	7	3	0.623
7/24/2008	0.655	0.75	0.11	7	4	3	0.401
7/25/2008	0.76	0.71	0.08	16	6	6	0.477
7/26/2008	0.83	0.90	0.08	2	4	5	0.766
7/27/2008	0.068	0.21	0.12	7	3	1	0.185
7/28/2008	0	−0.08	0.17	12	2	1	0.005
7/29/2008	0.081	0.14	0.08	9	1	0	0.097
7/30/2008	0	0.29	0.32	10	5	1	0.401
7/31/2008	0.05	0.14	0.09	11	2	0	0

[a] R^2 Values are also shown for the same regression statistics using the MOD04 collection 5 AOD product. Comparisons are between average midday AOD-predicted $PM_{2.5}$ concentrations and 10:00 A.M. to 2:00 P.M. LST average surface $PM_{2.5}$ concentrations.

Table 3.

Comparison of AOD-$PM_{2.5}$ Mean R^2 Values for the Developed AOD and MOD04 Collection 5 for Different Day Types

Day Type	This Study AOD-$PM_{2.5}$ mean R^2	MOD04 Collection 5 AOD-$PM_{2.5}$ mean R^2
Minimal impact (0 sites above 50 μg/m3 PM2.5)	0.05	0.04
Local impact (at least five sites above 50 μg/m3 PM2.5)	0.43	0.33
Widespread impact (at least 10 sites above 50 μg/m3 PM2.5)	0.48	0.23

Table 4.

Adjusted Regression Statistics for Comparisons of Predicted Surface $PM_{2.5}$ Concentrations to Measured Surface $PM_{2.5}$ By Site[a]

Site	R^2 (adj)	Slope	Intercept	R^2 (adj) Without 7/11	Slope Without 7/11	Intercept Without 7/11
Benicia	0.6	0.54	0	0.69	0.61	−1
Chico	0.5	0.49	27	0.52	0.52	27
Clovis	0.35	0.91	18	0.38	1.08	15
Colusa	0.61	0.6	5	0.68	0.66	2
Davis	0.54	0.38	10	0.82	0.55	1
Elk Grove	0.2	0.23	21	0.62	0.63	3
Folsom	0.46	0.37	23	0.73	0.55	18
Fresno	0.3	0.94	16	0.34	1.1	14
Grass Valley	0.44	0.67	6	0.44	0.67	6
Gridley	0.4	0.45	23	0.65	0.7	13
Livermore	0.45	0.65	2	0.66	0.95	−4
Lone Pine	0.59	0.16	6	0.59	0.16	6
Modesto	0.79	1.11	18	0.79	1.11	18
Napa	0.41	0.29	17	0.54	0.36	16
Portola	0.45	1.04	0	0.46	1.1	0
Quincy	0.72	1.67	12	0.72	1.67	12
Roseville	0.52	0.41	20	0.72	0.55	15
Sacramento Del Paso Manor	0.31	0.31	26	0.67	0.62	18
Sacramento T Street	0.29	0.28	21	0.71	0.6	12
San Jose	0.47	0.71	6	0.48	0.72	6
Stockton	0.52	0.68	0	0.74	0.93	−7
Truckee	0.17	0.57	15	0.17	0.57	15
Turlock	0.35	1.13	5	0.4	1.3	1
Vallejo	0.52	0.34	9	0.62	0.38	8
Willows	0.56	0.63	5	0.57	0.64	6
Yuba City	0.56	0.54	14	0.81	0.75	5
Minimum	0.17	0.16	0	0.17	0.16	−7
Mean	0.46	0.62	12.50	0.60	0.75	8.65

Site	R^2 (adj)	Slope	Intercept	R^2 (adj) Without 7/11	Slope Without 7/11	Intercept Without 7/11
Maximum	0.79	1.67	27	0.82	1.67	27

[a] Comparisons are between average midday AOD-predicted $PM_{2.5}$ and 10:00 A.M. to 2:00 P.M. LST average surface $PM_{2.5}$ concentrations.